

**Viscous Diffusion of Vorticity in
Unsteady Wall Layers Using the
Diffusion Velocity Concept**

J. H. Strickland
S. N. Kempka
W. P. Wolfe
Sandia National Laboratories
Albuquerque, NM 87185

**Forum on the Application of Vortex
Methods to Engineering Problems**

Sandia National Laboratories
Albuquerque, NM 87185-0836
February 22-24, 1995

MASTER

DISCLAIMER

Portions of this document may be illegible in electronic image products. Images are produced from the best available original document.

Viscous Diffusion of Vorticity in Unsteady Wall Layers Using the Diffusion Velocity Concept[†]

J. H. Strickland*, S. N. Kempka*,
and W. P. Wolfe*

*Engineering Sciences Center
Sandia National Laboratories
Albuquerque, NM 87185-0836*

ABSTRACT

The primary purpose of this paper is to provide a careful evaluation of the diffusion velocity concept with regard to its ability to predict the diffusion of vorticity near a moving wall. A computer code BDIF has been written which simulates the evolution of the vorticity field near a wall of infinite length which is moving in an arbitrary fashion. The simulations generated by this code are found to give excellent results when compared to several exact solutions. We also outline a two-dimensional unsteady viscous boundary layer model which utilizes the diffusion velocity concept and is compatible with vortex methods. A primary goal of this boundary layer model is to minimize the number of vortices generated on the surface at each time step while achieving good resolution of the vorticity field near the wall. Preliminary results have been obtained for simulating a simple two-dimensional laminar boundary layer.

INTRODUCTION

Background

Our ultimate reason for doing this work is to be able to develop a robust algorithm which is compatible with vortex methods while at the same time yielding good resolution of the vorticity/velocity field near the wall. Several attempts have been made in the past to couple inviscid vortex models with classical integral boundary layer formulations. Typical of these is the work due to Spalart and Leonard [1] and Spalart [2]. The integral solutions were started from a

known stagnation point and proceeded in the stream-wise direction until separation was indicated. Slightly upstream of the separation point, vortices were introduced to replace the vorticity in the boundary layer and were then allowed to convect freely in the flow. While the method gives good results for simple boundary layer flows, it is difficult (if not impossible) to apply to complicated unsteady flows in which there are multiple stagnation, separation, and reattachment points which are moving as a function of time.

There are several methods in which the viscous diffusion process (not necessarily in thin boundary layers) has been modeled using Lagrangian vortex elements. These methods include the Gaussian random walk method [3], the diffusing core method [4], the particle strength exchange (PSE) method [5], and the diffusion velocity method originally proposed by Ogami and Akamatsu [6] and improved by Kempka and Strickland [7]. The relative merits of these methods are discussed in [7].

Chorin [8] applied the "random walk" method to boundary layers utilizing vortex sheets near the wall. His method predicts a zero pressure gradient laminar boundary layer quite well but does not successfully predict separating boundary layers. This is probably due to his use of boundary layer assumptions near the separation point. For instance, the equation he used to calculate the stream-wise velocity as a function of distance from the wall neglects the stream-wise gradient of the normal velocity. Near the separation point this gradient is the same order of magnitude as the vorticity and cannot be neglected.

Koumoutsakos, Leonard, and Pepin [9] recently applied the PSE method to flow around both an oscillating and impulsively started circular cylinder. They obtained excellent results for the range of Reynolds numbers studied (40 to 10,000). It appears that the number of vortices N_v used in their work scales roughly as \sqrt{Re} . This scaling is consis-

[†] This work performed at Sandia National Laboratories supported by the U. S. Dept. of Energy under contract No. DE-AC04-94AL85000. Paper presented at the Forum on the Application of Vortex Methods to Engineering Problems, Sandia National Laboratories, Albuquerque, NM 87185, February 22-24, 1995.

* Senior Member Technical Staff

tent with the assumption that the thickness of the boundary layer δ , non-dimensionalized by a length L , scales as $1/\sqrt{Re}$ and that the overlapping vortex elements are circular. The primary disadvantage of the PSE method is that the region near the boundary must initially be flooded with vortex elements whose size, number, and extent must be judiciously chosen. As these elements convect in the flow, additional adjustments must be made in order to maintain a sufficient number of elements near the boundaries which are sized to properly resolve the boundary layer.

It should be noted at this point, that a topological problem exists if one tries to use circular vortex blobs to simulate boundary layers at high Reynolds Numbers. Consider a two-dimensional unsteady flow field which contains boundaries which are impenetrable. In order to solve the flow field, we first discretize the boundary into a number of curved or flat panels of length $O(h)$. From a knowledge of the existing vorticity field (which may be zero initially) and the motion of the boundaries we are then able to calculate the vorticity flux which must occur during the next time step to maintain the normal and tangential velocity boundary conditions. Our first inclination, in applying the vortex method to this problem, is to model the new vorticity generated at the wall by circular vortex blobs, preferably of diameter $O(h)$. However, for high Reynolds number flows, the vorticity will not diffuse away from the wall by a distance $O(h)$. If we nevertheless persist in placing overlapping circular blobs on the boundary at a distance away from the wall of $O(h)$, we are actually obtaining a solution for a lower local Reynolds number. In order to accurately model the diffusion process using circular blobs, we must place a large number of overlapping circular vortices along the wall whose diameters will be some fraction of the boundary layer thickness. For high Reynolds number flows the boundary layer thickness may itself be some fraction of h . In such cases, the number of vortex blobs required becomes prohibitive. We note that Chorin's use of vortex sheets in reference [8] was motivated by this very problem which became apparent in his earlier work [3] in which he used circular vortex blobs with finite cores.

General Methodology

We now outline a two-dimensional unsteady viscous boundary layer model which is compatible with vortex methods. We first define two regions, a wall region for $y \leq h$ and an outer region for $y > h$ where y is the normal distance away from the wall and h is the local panel length. It is assumed that the boundary is properly paneled in order to resolve the wall boundary conditions. In the wall region, elements used to represent the vorticity field must be elongated in the stream-wise direction as compared with their thickness normal to the wall. In the outer region, the vortex elements are circular with diameters of $O(h)$. In the wall region, diffusion may be assumed to be unidimensional so

long as the wall curvature is not too severe while in the outer region diffusion will be considered as two-dimensional. Finally, in the wall region, a Lagrangian re-map scheme is used to obtain the evolution of the vorticity field while in the outer region a viscous vortex blob method is used. The vortex elements defined in each region are able to smoothly interact with the elements of the other region or transition from one region to the other. This method is intended to yield good resolution of the diffusion and convection processes for $y \leq h$ without generating any "free" vortex blobs which are smaller than $O(h)$.

The general solution scheme for the wall region is to first diffuse vorticity into the layer, allow diffusion of the existing vorticity to occur, convect the flow, re-map the vorticity distribution back onto lines normal to the wall which are spaced at intervals h , and repeat for the next time step. In most regions of high Reynolds number boundary layer flows only the wall region will be required since the diffusing layer will not extend beyond $y = h$. For cases where sufficient vorticity moves across $y = h$ we convert the vorticity into "free" circular vortex blobs of support $O(h)$. Conversely, vortex blobs may penetrate the wall layer in which case the vorticity from such blobs is "captured" and placed in the wall layer.

As mentioned previously, the vorticity flux which moves through the wall during a given time step is obtained by enforcing the normal and tangential velocity boundary conditions. A first order approach is to assume that the vorticity is impulsively introduced into the layer at the middle of each time step. Koumoutsakos, Leonard, and Pepin [9] developed a method which allows one to calculate the two-dimensional distribution of this new vorticity in the region near the wall. For unidimensional diffusion, the distribution of new vorticity is identical with the distribution of vorticity for an impulsively started flat plate. We will expand upon this topic in the section "Generation of Vorticity at the Wall" on page 4.

The diffusion process is modeled by using one-dimensional overlapping linear vortex elements as indicated in Figure 1. It is possible to use other one-dimensional vortex elements in this region such as Gaussian or "skewed" Gaussian elements (i. e. different core radii for positive and negative positions with respect to the element center). However, the linear elements provide a much simpler model and do not suffer from typical problems near walls of distributions which do not have compact support (i.e. part of the distribution extends across the wall). These elements diffuse according to the "diffusion" velocity \bar{u}_d at their edges and center. In order to conserve circulation strength, the area of each triangle under the ω, y curve remains constant as a function of time. Details of the diffusion velocity concept will be given in the section "The Diffusion Velocity Concept" on page 3.

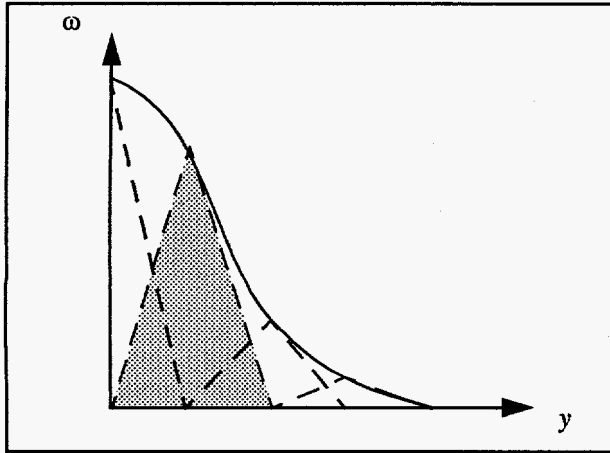


Figure 1. Typical Wall Layer Diffusion Elements

Our next task is to convect the flow in the wall layer. For convection purposes we use quadrilateral Lagrangian elements as shown in Figure 2. Due to the rapid distortion of the elements in the wall layer (especially next to the wall), the vorticity distribution is re-mapped at each iteration back onto lines which are normal to the wall.

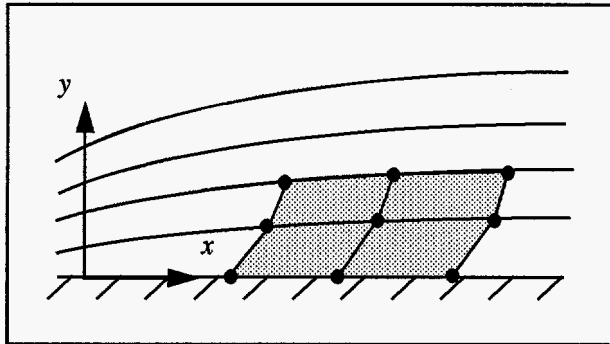


Figure 2. Typical Wall Layer Convection Elements

The tangential convection velocity may be obtained from the following equation which is based upon the definition of vorticity in terms of velocity.

$$u = u_w - \int_w^y \omega dy + \int_w^y \frac{\partial v}{\partial x} dy. \quad (1)$$

The normal component of the convection velocity may be obtained from the continuity equation as:

$$v = v_w - \int_w^y \frac{\partial u}{\partial x} dy. \quad (2)$$

For most regions of the wall layer (away from separation or reattachment points) the last integral in Equation 1 is negligible. This allows one to obtain solutions to Equations 1 and 2 in a very simple manner, solving first for u in terms of the known vorticity distribution normal to the wall and then for v in terms of the local stream-wise gradient of u . For regions where the last integral in Equation 1 cannot be neglected, several options have been examined which will be presented in a future paper. In each of the options, we plan to use local information in the formulation which negates the need to perform calculations in this layer which requires information directly from all of the other vortex elements and vortex blobs in the global flow field.

In the outer region ($y > h$), the flow is modeled by two-dimensional vortex blobs. The centers of the vortices are convected at a velocity which is the sum of the local diffusion velocity and the local fluid velocity. In addition, the core radii of the vortices expand to account for the non-solenoidal nature of the diffusion velocity (see reference [7]). We thus invoke the Biot-Savart law and the diffusion velocity concept to obtain the velocity and core expansion rate of each vortex. To reduce the computation time from order N_V^2 to order N_V or $N_V \ln N_V$, where N_V is the number of free vortices, we use the fast adaptive multipole method due to Carrier, Greengard, and Rokhlin [10].

In closing this section, we acknowledge that the above outline which we have given for the solution of two-dimensional boundary layers using a vortex method is very sketchy. As stated earlier, the primary work presented in this report concerns the simulation of viscous diffusion in the wall layer using the diffusion velocity concept. Our purpose for including the above outline is to orient the reader to the role which the diffusion sub-model will play in a more general scheme. In the following sections, we will describe in some detail the method of solution associated with the diffusion process in the wall layer.

METHOD OF SOLUTION

The Diffusion Velocity Concept

In order to illustrate the diffusion velocity concept, consider the two-dimensional viscous flow field depicted in Figure 3. The diffusion velocity is specified such that the circulation within a given boundary remains constant if that boundary moves at the diffusion velocity plus the local fluid velocity. In order to formulate the diffusion velocity we first note that the circulation around a curve enclosing an area A is:

$$\Gamma = \int_A \vec{\omega} \cdot \hat{n} dA. \quad (3)$$

Taking the time derivative of Equation 3 and setting it equal to zero yields:

$$\frac{d\Gamma}{dt} = 0 \quad (4)$$

or

$$\int_A \left[\frac{\partial}{\partial t} \vec{\omega} + (\vec{u} \cdot \nabla) \vec{\omega} + \vec{\omega} (\nabla \cdot \vec{u}) - (\vec{\omega} \cdot \nabla) \vec{u} \right] \cdot \hat{n} dA = 0$$

where \vec{u} is the velocity at which the area A is moving. We now let $\vec{u} = \vec{u} + \vec{u}_d$, where the local fluid velocity is \vec{u} and the local diffusion velocity is \vec{u}_d .

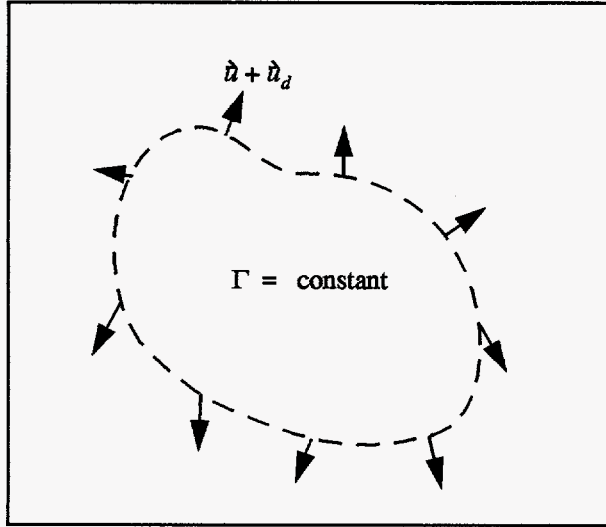


Figure 3. Diffusion Velocity Concept

Equation 4 is satisfied when the integrand is equal to zero:

$$\frac{\partial}{\partial t} \vec{\omega} + (\vec{u} \cdot \nabla) \vec{\omega} + \vec{\omega} (\nabla \cdot \vec{u}) - (\vec{\omega} \cdot \nabla) \vec{u} = 0. \quad (5)$$

We also have at our disposal the vorticity form of the Navier-Stokes equation:

$$\frac{\partial}{\partial t} \vec{\omega} + (\vec{u} \cdot \nabla) \vec{\omega} + \vec{\omega} (\nabla \cdot \vec{u}) - (\vec{\omega} \cdot \nabla) \vec{u} = \nu \nabla^2 \vec{\omega}. \quad (6)$$

Subtracting Equation 6 from Equation 5 yields the governing equation for the diffusion velocity in terms of the vorticity field and kinematic viscosity:

$$(\vec{u}_d \cdot \nabla) \vec{\omega} + \vec{\omega} (\nabla \cdot \vec{u}_d) - (\vec{\omega} \cdot \nabla) \vec{u}_d = -\nu \nabla^2 \vec{\omega}. \quad (7)$$

Using the vector identities,

$\nabla \times (\nabla \times \vec{\omega}) = \nabla (\nabla \cdot \vec{\omega}) - \nabla^2 \vec{\omega}$, $\nabla \cdot \vec{\omega} = 0$, and $\nabla \times (\vec{u}_d \times \vec{\omega}) = (\vec{\omega} \cdot \nabla) \vec{u}_d - (\vec{u}_d \cdot \nabla) \vec{\omega} + \vec{u}_d (\nabla \cdot \vec{\omega}) - \vec{\omega} (\nabla \cdot \vec{u}_d)$, Equation 7 can be written in a form in which the diffusion velocity appears only once,

$$-\nabla \times (\vec{u}_d \times \vec{\omega}) = \nu \nabla \times (\nabla \times \vec{\omega}). \quad (8)$$

This equation implies that to within an arbitrary constant:

$$\vec{u}_d \times \vec{\omega} = -\nu \nabla \times \vec{\omega}. \quad (9)$$

The arbitrary constant can be shown to be equal to zero. We now restrict ourselves to two dimensions and rewrite Equation 9 as:

$$\vec{u}_d = -\frac{\nu}{\omega} \nabla \omega, \quad (10)$$

where ω is the vorticity which is perpendicular to the two-dimensional plane. In order to determine the time rate of change of the vorticity as we move along at the velocity \vec{u} (denoted by $\tilde{D}/\tilde{D}t$) we write Equation 5 for the two-dimensional case:

$$\frac{\tilde{D} \vec{\omega}}{\tilde{D} t} = -\vec{\omega} (\nabla \cdot \vec{u}) = -\vec{\omega} (\nabla \cdot \vec{u}_d). \quad (11)$$

We see from this equation that the time rate of change of vorticity is a function of the divergence of the diffusion velocity since $\nabla \cdot \vec{u} = 0$ for incompressible flow.

Since we are dealing with boundary layers, the diffusion in the direction tangential to the wall (the x direction) may be ignored. Thus we only concern ourselves with the diffusion velocity in the direction normal to the wall (the y direction) which will be denoted by U_d .

$$U_d = -\frac{\nu}{\omega} \frac{\partial \omega}{\partial y}. \quad (12)$$

The evolution equation for ω may be obtained from Equation 11 as:

$$\frac{\tilde{D} \omega}{\tilde{D} t} = -\omega \frac{dU_d}{dy}. \quad (13)$$

We will also be interested in the flux of circulation γ per unit length of x across some point y . This flux is simply the product of the diffusion velocity and the vorticity or:

$$\frac{\partial \gamma}{\partial t} = -\nu \frac{\partial \omega}{\partial y}. \quad (14)$$

In summary, Equations 12, 13, and 14 form the set of equations which we will use for solution of the viscous diffusion in the region near the wall.

Generation of Vorticity at the Wall

The circulation per unit length γ which must be generated at the wall in order to maintain the no-slip condition is

equal to the slip velocity U_s which becomes manifest at a particular location on the wall during a time period Δt . A generalized method to obtain U_s (or γ on the wall) is given in reference [12]. In order to gain insight into the actual distribution of vorticity, we begin by examining a point on a moving boundary in a time dependent flow. We assume that initially the fluid velocity is equal to zero relative to the selected point on the wall and we examine the nature of the slip velocity over a short period of time Δt . As fluid is convected from other points in the flow over the point on the wall there is no reason to expect that the fluid velocity relative to the point on the wall will remain zero unless we introduce vorticity into the flow. For example, we may have stream-wise pressure gradients along the wall. This causes the circulation in the boundary layer which is convecting from upstream to either be too high or too low to produce a zero slip velocity at the wall. In addition, the wall itself might be moving in an unsteady fashion. We can define the wall slip velocity U_s which will arise over a time Δt (barring any flux of vorticity through the wall) as:

$$U_s = U_{ws} - U_{wf} \quad (15)$$

where U_{ws} is the tangential surface velocity or tangential velocity boundary condition and U_{wf} is the tangential fluid velocity which are both positive in the direction of the unit surface tangent vector $\vec{\tau}_s$. In order to restore the no-slip condition at the wall during the increment of time Δt , a flux of vorticity must occur through the wall into the fluid. This flux can be written in terms of the diffusion velocity U_d and the wall slip velocity U_s as:

$$\omega U_d \Delta t = \Delta U_s \quad (16)$$

or

$$\omega U_d = \frac{dU_s}{dt} \quad (17)$$

We notice that Equation 17 is simply an application of Equation 14 with $\gamma = U_s$. It should be noted that if the surface normal vector which is pointing into the flow of interest is $\vec{\eta}_s$, the positive direction associated with $\vec{\omega}$ in Equation 17 is given by $\vec{\tau}_s \times \vec{\eta}_s$. Since the diffusion velocity U_d at the wall is given by:

$$U_d = -\frac{v}{\omega} \frac{\partial \omega}{\partial y} \Big|_w \quad (18)$$

then the vorticity gradient at the wall is given by:

$$\frac{\partial \omega}{\partial y} \Big|_w = -\frac{1}{v} \frac{dU_s}{dt} \quad (19)$$

It should be pointed out that an interpretation of Equation 19 can be obtained directly from the two-dimensional boundary layer form of the Navier-Stokes equations. The two-dimensional boundary layer form of the Navier-Stokes equations can be written as:

$$\frac{\partial u}{\partial t} + u \frac{\partial u}{\partial x} + v \frac{\partial u}{\partial y} = -\frac{1}{\rho} \frac{dp}{dx} + \nu \frac{\partial \omega}{\partial y} \quad (20)$$

By comparing Equation 19 with Equation 20 evaluated at the wall it can be seen that the time rate of change of the wall slip velocity is equivalent to the combined effects of the pressure gradient term and the wall surface motion. It is also clear that Equation 19 is much more convenient for calculating the normal gradient of the vorticity at the wall when using vorticity methods as compared to Equation 20 evaluated at the wall.

We have examined several numerical models for introducing the vorticity into the flow at the wall. The simplest method is to add all of the circulation which is generated at the wall during a given time step to the first linear vortex element next to the wall (the right triangle next to the wall in Figure 1) and then allow the entire distribution to diffuse over the time step. There are a number of variations on this basic scheme in which the vorticity is introduced in smaller amounts on more than one occasion during the time step. In a recent paper by Koumoutsakos, Leonard, and Pepin [9] concerning vorticity generation at a wall, an algorithm for updating the particle strengths in a PSE method was presented for finite panels with curvature. In the context of the present unidimensional model, the vorticity which would be introduced into the domain from the wall during a time Δt would have a distribution equal to:

$$\Delta \omega = \omega^{t+\Delta t} - \omega^t = \frac{U_s e^{-\frac{y^2}{4\nu\Delta t}}}{\sqrt{\pi\nu\Delta t}} \quad (21)$$

where $\omega^{t+\Delta t}$ is the vorticity at the time $t + \Delta t$ and ω^t is the vorticity at time t . We note that Equation 21 is identical to the exact solution for an impulsively started flat plate [11]. Adding all of the circulation to the first element at the beginning of the time step is roughly equivalent to using Equation 21 at the end of the time step.

Since the diffusion equation is linear, we may obtain the vorticity distribution associated with the flux from the wall at the end of the time step by superimposing the impulsive solutions via the following convolution integral.

$$\Delta \omega = \int_0^{\Delta t} \frac{\partial U_s}{\partial \tau} \frac{\exp\left(-\frac{y^2}{4\nu(\Delta t - \tau)}\right)}{\sqrt{\pi\nu(\Delta t - \tau)}} d\tau \quad (22)$$

Defining $y^+ = y/\sqrt{\nu t}$, Equation 22 can be integrated numerically to obtain the curve shown in Figure 4 which is labeled as "Exact". The resulting distribution can be fitted with a curve given by:

$$\Delta\omega^+ = \frac{\Delta\omega\sqrt{\frac{\nu}{\Delta t}}}{\frac{\partial U_s}{\partial \tau}} = 1.131e^{-q} \quad (23)$$

where

$$q = 0.884y^+ + 0.161y^{+2} \quad (24)$$

For comparison, the distribution given by a single impulse at the mid time step is also plotted in Figure 4 identified in the legend by $0.5\Delta t$. The major difference in the two curves is their distributions near the wall. From Equation 19 it is seen that the slope of the $(\Delta\omega^+, y^+)$ curve at the wall must be equal to minus one, not zero as is given by the impulsive start representation. We note that the proper slope is obtained when using Equation 23.

For simulations where $\Delta t \Rightarrow 0$, the global vorticity distribution will tend to be the same for the various representations of the wall flux distribution. On the other hand, we have found that one has to sometimes take much smaller time steps when using the impulsive representation in order to obtain satisfactory distributions near the wall. we therefore recommend the use of Equation 23.

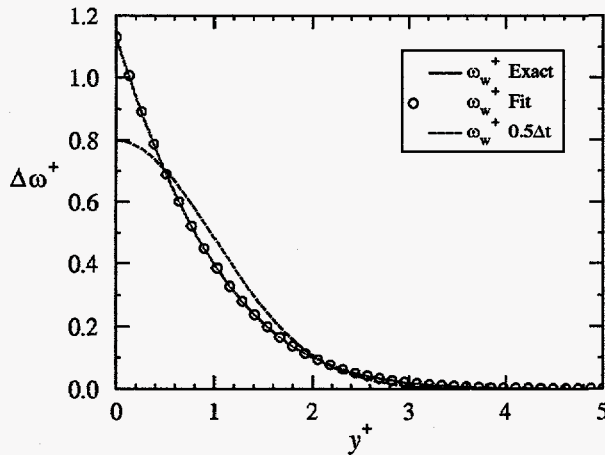


Figure 4. Distribution of Wall Vorticity

The Diffusion Velocity for Zero Vorticity

In order to use Equation 12, it is important to obtain an understanding of its behavior for the case where $\omega = 0$. We note that there are two basic zero vorticity cases which

must be considered. In the first case, the vorticity and its slope are both approaching zero. In the second case, the vorticity is zero but the slope is non-zero.

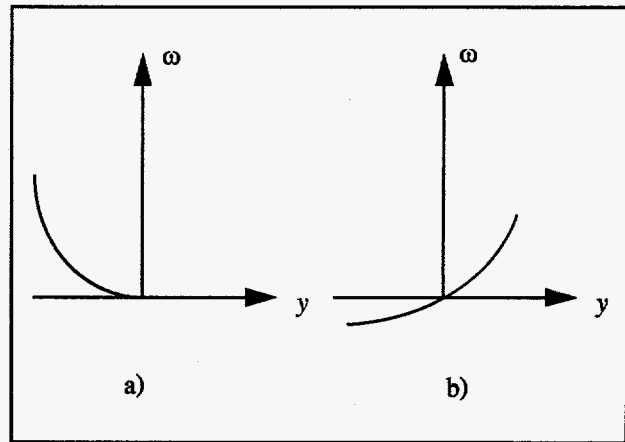


Figure 5. Zero Vorticity Cases

We first examine the case shown in Figure 5a. The diffusion velocity in the region where $\omega \rightarrow 0$ is indeterminate for this case since $\partial\omega/\partial y$ is also approaching zero. In order to form a numerical model for this case, we assume a linear vorticity distribution as shown in Figure 6. Since our primary interest is in the diffusion of this linear element, we write an equation for the mean diffusion velocity U_{dM} at $y = h/2$ and equate that to the average of the diffusion velocities at the ends of the element.

$$U_{dM} = \frac{U_{dL} + U_{d0}}{2} = -\frac{2\nu}{\omega_L} \left(-\frac{\omega_L}{h} \right). \quad (25)$$

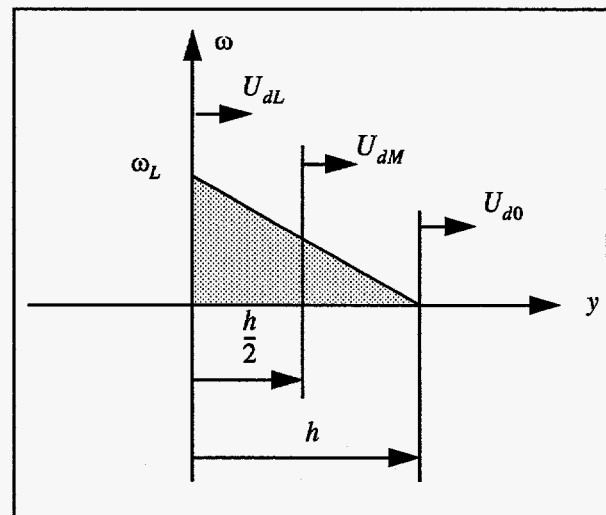


Figure 6. Diffusion Velocity For Zero Vorticity and Vanishing Slope.

Solving Equation 25 for U_{d0} yields:

$$U_{d0} = 4\frac{v}{h} - U_{dL}. \quad (26)$$

To test the applicability of Equation 26, we examine its predictive quality with regard to diffusion of vorticity in a flow in which the wall is impulsively started from rest to a velocity of U_e , sometimes referred to as "Stokes' first problem" [11]. We will model the entire vorticity field with a single linear element, realizing that this is a very crude model for such a flow. In an actual simulation, this linear element would represent only a small region of the flow at the edge of the boundary layer. In Figure 6, we place the wall at $y = 0$ and let ω_L be equal to the vorticity at the wall. Recasting Equation 26 in terms of the time rate of change of h , we obtain:

$$\frac{dh}{dt} = 4\frac{v}{h} - U_{dL}. \quad (27)$$

In modeling an impulsively started flow, U_{dL} will be equal to zero since the wall boundary condition dictates that $\partial\omega/\partial y = 0$ for $y = 0$ and $t > 0$. We enforce this boundary condition without regard for the fact that $\partial\omega/\partial y \neq 0$ for $y > 0$. Therefore, Equation 27 can be integrated to yield h as a function of time with the initial condition that $h = 0$ when $t = 0$:

$$h = 2\sqrt{2vt}. \quad (28)$$

The vorticity distribution can now be written as:

$$\frac{\omega\sqrt{vt}}{U_e} = \frac{1}{\sqrt{2}} \left[1 - \frac{1}{\sqrt{2}} \left(\frac{y}{2\sqrt{vt}} \right) \right], \quad (29)$$

where $U_e = \omega_L h/2$ is the velocity of the impulsively started plate. The exact solution for the vorticity distribution is given by:

$$\frac{\omega\sqrt{vt}}{U_e} = \frac{1}{\sqrt{\pi}} \exp\left(-\frac{y^2}{4vt}\right). \quad (30)$$

Equations 29 and 30 are plotted in Figure 7. As may be seen from this figure, the vorticity distribution obtained from the one element linear approximation is surprisingly close to that of the exact solution and in fact, fluid velocity profiles obtained by integrating these curves would appear to be even more similar. Based on this limited test, we conclude that Equation 26 will probably give satisfactory results for representing an element (in a general numerical model) where ω and $\partial\omega/\partial y$ are both approaching zero.

Next, consider the case depicted in Figure 5b in which $\omega = 0$ but $\partial\omega/\partial y \neq 0$. From Equation 12, it may be seen that there is a jump in the value of U_d from a very large

positive value to a very large negative value as one moves from left to right across the ω axis along the y axis. This indicates that negative vorticity is flowing to the right while positive vorticity flows to the left across the origin. The strength γ_{2h} of the vortex sheet between $y = \pm h$ is constant with respect to time, since those boundaries are moving at their respective diffusion velocities. The vorticity sheet strength γ_R for the right hand layer ($0 \leq y \leq h$) is decreasing, on the other hand, at a rate given by:

$$\frac{d\gamma_R}{dt} = -v \frac{\partial\omega}{\partial y}, \quad (31)$$

The vorticity sheet strength γ_L for the left hand layer ($h \leq y \leq 0$) is increasing (in a positive sense) at an equal rate. Thus, we observe that positive and negative vorticity is being destroyed in equal amounts. We also note that the absolute values of the strengths for the left and right hand sheets are decreasing in equal amounts as the elements collapse toward the origin.

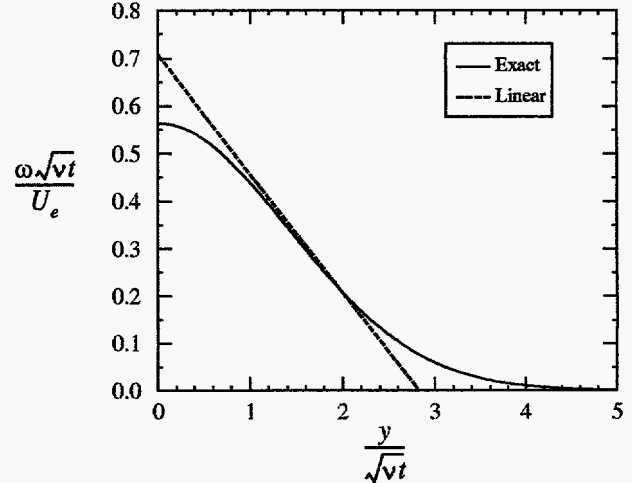


Figure 7. One Element Linear Approximation To "Stokes First Problem."

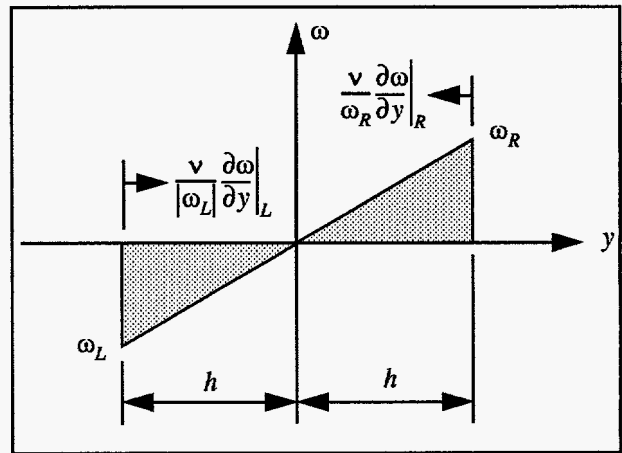


Figure 8. Zero Vorticity With Non-zero Slope

We now turn to the calculation of the velocity of the point $(y, \omega) = (0, 0)$. The approach that we take is to obtain an average or integral value of the diffusion velocity for the "element" between $y = \pm h$ and then take the limit as $h \rightarrow 0$. The average diffusion velocity U_{d0} for this element can be written as:

$$U_{d0} = -\frac{v}{2h} \left(\frac{2}{\omega_R} \frac{\partial \omega}{\partial y} \Big|_R + \frac{2}{\omega_L} \frac{\partial \omega}{\partial y} \Big|_L \right) h. \quad (32)$$

Noting that $\omega_L \cong -\omega_R$ and that the equality will be true as $h \rightarrow 0$, Equation 32 can be rewritten as:

$$U_{d0} = -\frac{v}{\omega_R} \left(\frac{\partial \omega}{\partial y} \Big|_R - \frac{\partial \omega}{\partial y} \Big|_L \right) \frac{1}{h}. \quad (33)$$

Taking the limit $\lim_{h \rightarrow 0} U_{d0}$ yields:

$$U_{d0} = -\frac{v}{\frac{\partial \omega}{\partial y}} \left(\frac{\partial^2 \omega}{\partial y^2} \right). \quad (34)$$

Equation 34 could have also been obtained by a L'Hospital type of differentiation of the numerator and denominator of Equation 12, although the nature of the singularities for this case do not appear to fit the L'Hospital rules. It should be noted that U_{d0} is not, strictly speaking, a diffusion velocity but is the velocity of the point at which $\omega = 0$ when $\partial \omega / \partial y \neq 0$. As noted previously, the individual strengths of the vortex sheets on either side of this point are not conserved and must be adjusted according to Equation 31 and its counterpart for the left hand layer. This point moves in response to the local curvature in the (y, ω) curve and always moves in a direction so as to reduce the curvature.

In order to test the validity of Equation 34, we examined the solution to "Stokes' second problem" [11] which is an exact solution for viscous flow near a sinusoidally oscillating infinite flat plate. The velocity profile for this problem is given by:

$$\frac{u(y, t)}{U_o} = \exp\left(-\sqrt{\frac{n}{2\nu}} y\right) \cos\left(nt - \sqrt{\frac{n}{2\nu}} y\right), \quad (35)$$

where U_o is the maximum velocity at the wall and n is the frequency of oscillation. The vorticity field is given by:

$$\frac{\omega(y, t)}{U_o} = \quad (36)$$

$$\sqrt{\frac{n}{2\nu}} \exp\left(-\sqrt{\frac{n}{2\nu}} y\right) \left[-\cos\left(nt - \sqrt{\frac{n}{2\nu}} y\right) + \sin\left(nt - \sqrt{\frac{n}{2\nu}} y\right) \right]$$

For $\omega = 0$ we see that the argument of the trigonometric functions must be equal to a constant (either $\pi/4$ or $5/4\pi$). The velocity of the point where $\omega = 0$ is then obtained by differentiating the argument of the trigonometric functions to obtain:

$$\frac{dy}{dt} \Big|_{\omega=0} = \sqrt{2\nu n}. \quad (37)$$

In order to test Equation 34 against this result, we obtain the first and second derivatives of ω from Equation 36 and insert their values with $\omega = 0$ into Equation 34. This yields:

$$U_{d0} = -\frac{v}{\frac{\partial \omega}{\partial y}} \left(\frac{\partial^2 \omega}{\partial y^2} \right) = \sqrt{2\nu n}, \quad (38)$$

which of course is the same result as that obtained for the motion of the point where $\omega = 0$.

Another way to avoid having to make calculations for the case shown in Figure 5b, altogether, is to break the vorticity distribution up into positive and negative distributions, diffuse them independently, and then add them back together. This is permissible since the diffusion process is linear. The cancellation of positive and negative vorticity occurs during the addition process and does not otherwise have to be accounted for. We found this method to be much more robust than that of the previous sections and have used it in all of our calculations.

The Numerical Model

The computer code BDIF simulates the vorticity and velocity field for viscous laminar flow over a moving wall of infinite extent with an arbitrary tangential motion. This model is also applicable to flow regions which are not too close to the ends of a finite length oscillating plate whose time integrated tangential velocity is equal to zero.

At time $t = 0$ one may specify an initial vorticity distribution. If there is an initial vorticity distribution it is first discretized into a number of linear blob elements as shown in Figure 1. Next, the distribution is expanded to include an image distribution for $y < 0$. This symmetry insures that no vorticity flows across the wall during the diffusion process associated with the initial distribution. The symmetrical distribution is then segmented into segments whose end points are the roots ($\omega = 0$) of the distribution. Segments which contain a zero vorticity distribution are discarded. Each node of the segment is moved according to either Equation 12 or 26. The discrete form of Equation 12 at node j is given by:

$$U_{d(j)} = -\frac{\nu}{2\omega_j} \left(\frac{\omega_j - \omega_{j+1}}{y_j - y_{j+1}} + \frac{\omega_j - \omega_{j-1}}{y_j - y_{j-1}} \right). \quad (39)$$

The discrete forms for the left and right ends of the distributions where $\omega = 0$ are given by:

$$U_{d(1)} = -\frac{4\nu}{y_2 - y_1} - U_{d(2)}$$

and

$$U_{d(n)} = \frac{4\nu}{y_n - y_{n-1}} - U_{d(n-1)}$$

respectively, where n is the last node in the distribution. Each node is then transported to a new location using a simple Euler time integration of the equation given by:

$$\frac{dy_j}{dt} = U_{d(j)}. \quad (41)$$

Equation 13 is then satisfied by maintaining a constant area with respect to time in each of the linear blobs as depicted in Figure 1. The discrete equation is given by:

$$\omega_j^{t+\Delta t} (y_{j+1}^{t+\Delta t} - y_{j-1}^{t+\Delta t}) = \omega_j^t (y_{j+1}^t - y_{j-1}^t) \quad (42)$$

Next, the segments are added back together and the symmetrical distribution is reduced to a one-sided distribution ($y \geq 0$). This then represents the distribution of the vorticity which was present at the beginning of the time step in its diffused state at the end of the time step.

Since the diffusion problem is linear, we may allow the vorticity generated at the wall to diffuse independently over the course of the time step. Thus, we simply add the distribution of wall generated vorticity given by Equation 23 to that of the diffused initial vorticity as calculated previously. The resulting vorticity distribution now becomes the initial vorticity distribution for the next time step.

NUMERICAL RESULTS

Initially Uniform Vorticity Sheet

An infinite plate moves at a constant velocity of U_e to the left. Initially, at time $t = 0$, we assume that the velocity profile is as shown in Figure 9. This profile is that of plane Couette flow. We do not concern ourselves with how this profile might have been generated but simply specify it as an initial condition. The linear velocity between $y = 0$ and $y = h$ at $t = 0$, implies that there is a layer of vortic-

ity of thickness h next to the surface. The vorticity in this layer is constant and has a value of $\omega = U_e/h$ in the clockwise direction. The governing equation for the vorticity is given by:

$$\frac{\partial \omega}{\partial t} = \nu \frac{\partial^2 \omega}{\partial y^2}. \quad (43)$$

For a constant plate velocity, the slip velocity at the surface is zero. Equation 19 then yields the following boundary condition for Equation 43:

$$\frac{\partial \omega}{\partial y} = 0 \text{ for } y = 0. \quad (44)$$

Equation 44 used in conjunction with Equation 14 implies that no additional vorticity is being transported across the wall for $t > 0$ which we know to be true since the circulation in the boundary layer for $t \geq 0$ must remain constant in order to satisfy the no-slip condition.

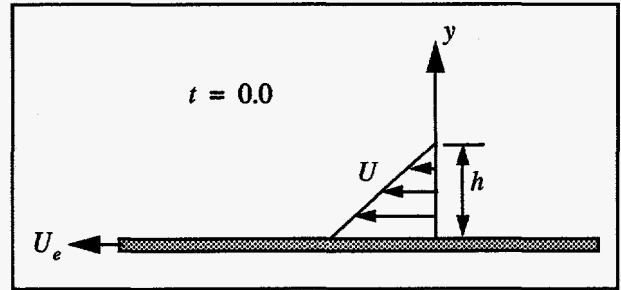


Figure 9. Initial Velocity Profile (Uniform Vorticity Sheet)

An exact analytical solution can be obtained for Equation 43 subject to the indicated initial and boundary conditions. This solution is given by:

$$\omega^* = \frac{1}{2} \left[\operatorname{erf} \left(\frac{1-y^*}{2\sqrt{t^*}} \right) + \operatorname{erf} \left(\frac{1+y^*}{2\sqrt{t^*}} \right) \right], \quad (45)$$

where, $\omega^* = \omega h/U_e$, $y^* = y/h$, and $t^* = \nu t/h^2$.

Plots of the vorticity distribution as a function of time using the computer code BDIF are given in Figure 10. The "exact" solution (Equation 45) is also plotted in Figure 10. We have removed approximately 50% of the points calculated by BDIF to enable one to be able to compare with the exact solution. The results using the diffusion velocity are seen to be in excellent agreement with the analytical results. The biggest error occurs at the edge of the boundary layer where ω is small and the diffusion velocity is large.

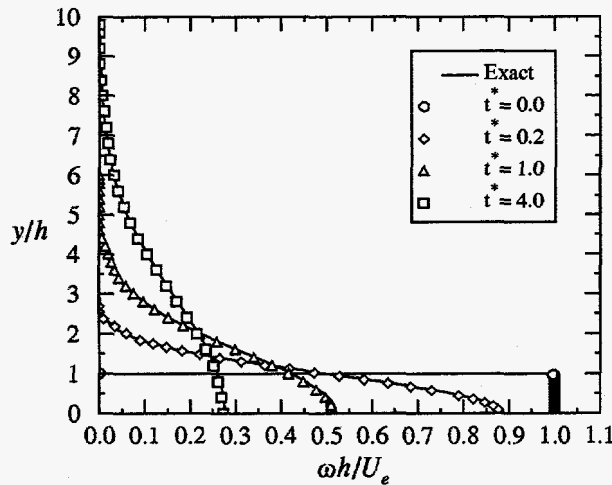


Figure 10. Vorticity Distributions as a Function of Time (Initially Uniform Vorticity Sheet)

Impulsively Started Plate

We next examine the impulsively started plate sometimes referred to as "Stokes' First Problem." The exact solution for the velocity distribution can be obtained from Currie [11]:

$$\frac{u}{U_e} = 1 - \operatorname{erf}\left(\frac{y}{2\sqrt{\nu t}}\right). \quad (46)$$

By differentiating Equation 46 with respect to y , the vorticity field is readily obtained:

$$\frac{\omega\sqrt{\nu t}}{U_e} = \frac{1}{\sqrt{\pi}} \exp\left(-\frac{y^2}{4\nu t}\right). \quad (47)$$

As a matter of interest, we replot the data for $t > 0$ from Figure 10 in Figure 11 along with the impulsive exact solution (Equation 47). As can be seen from this figure, for non-dimensional times t^* greater than 1.0 the vorticity profiles begin to approach that of an impulsively started plate.

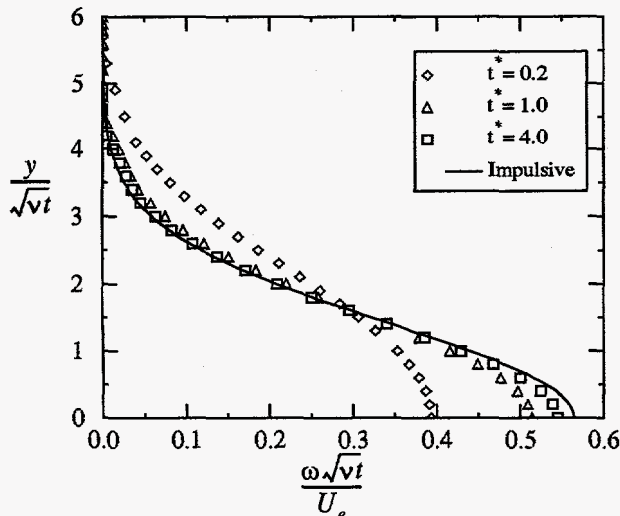


Figure 11. Vorticity Profiles for Impulsively Started Plate versus Initially Uniform Sheet

In order to simulate an impulsive start using the code BDIF we could simply run the uniform vorticity sheet case to large values of t . One suspects that the exact nature of the initial vorticity profile is unimportant at large times. In Figure 12 we show a calculation using BDIF in which the plate was accelerated from a zero velocity to the velocity U_e in a time step that is equal to $0.001t$. The exact calculation (Equation 47) is plotted for comparison. Again, we have removed approximately 50% of the points calculated by BDIF. These results show excellent agreement between the exact solution and the BDIF calculation.

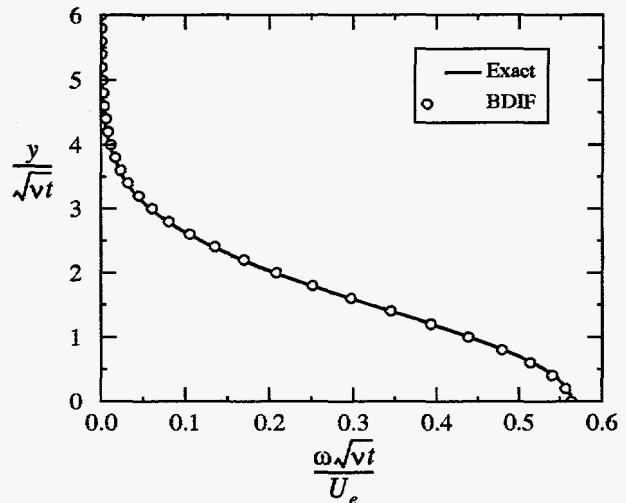


Figure 12. Vorticity Profile for Impulsively Started Plate

Sinusoidally Moving Plate

We next examine the sinusoidally oscillating plate which is sometimes referred to as "Stokes Second Problem." We have already noted the exact solution for the periodic state (Equation 36). Wu et. al. [13] and Panton [14] address the issue of transient vorticity values for this problem. By "transient" we mean the start-up period prior to a periodic solution.

One method of solving both the transient and periodic problem, is to use the convolution integral given by Equation 22. It can be noted that this integral is simply the convolution of the time rate of change of the slip velocity with a unit impulsive start solution. We have developed a simple computer code to numerically integrate this equation and refer to this method as the convolution integral method or CIM. Vorticity profiles are given in Figure 13 for three phase angles associated with the periodic solution. In order to insure that a periodic state was reached, the simulation covered about 500 cycles. The agreement between the exact solution and the CIM simulation which is denoted by the symbols is seen to be quite good.

In Figure 14 we compute the vorticity profiles in the eleventh cycle of oscillation. In this figure the CIM simulations form our baseline calculations and are denoted by the solid lines. The BDIF code was used to produce the data denoted by the symbols. The agreement is seen to be very good. It is interesting to note that while the character of Figure 14 is the same as that of Figure 13, the transient effects still linger after 10 cycles.

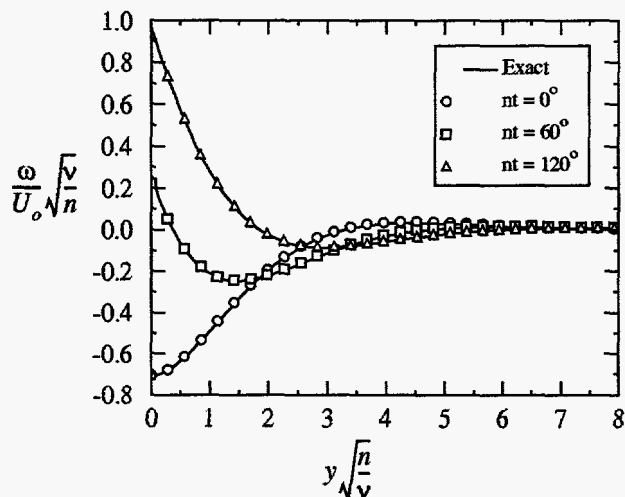


Figure 13. Periodic Vorticity Profiles for Sinusoidally Oscillating Plate

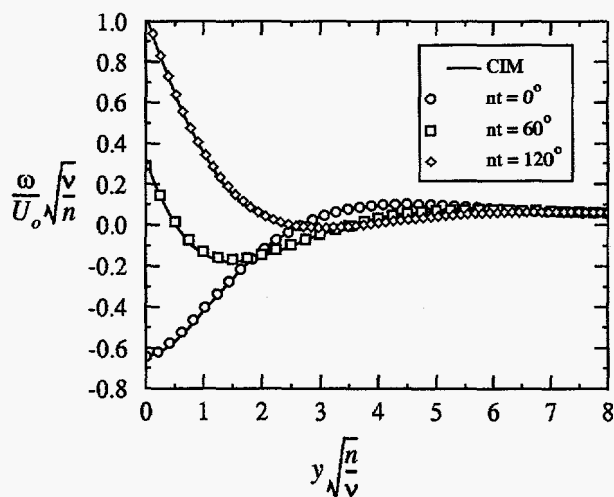


Figure 14. Vorticity Profiles after 10 Cycles for Sinusoidally Oscillating Plate

Blasius Solution

The last solution which we will examine is the case for flow over a finite length flat plate. This solution was generated by the code WALLYR which represents an exploratory im-

plementation of the boundary layer solver outlined in the section "General Methodology" on page 2. In this particular calculation, the size of the wall computational space and Reynolds number were chosen to contain all of the vorticity within the wall region ($y \leq h$) and, hence, there was no need for any of the vorticity to be represented by free two-dimensional blobs. Rather, we treat the entire boundary layer as a wall flow in which vorticity is introduced at the wall, diffused, and convected. The plate was descretized into 50 elements with $h = 1$.

The solution was started with the plate moving to the left with a velocity of $U_o = 1$. The initial vorticity distribution was assumed to be uniform along the length of the plate and was computed using Equation 21 with $\Delta t = 1$. Numerical experimentation revealed, however, that the starting solution did not affect the final results. For the results shown here, the solution converged at a non-dimensional time $t = 200$.

The results of the calculations for a Reynolds number based on the length from the plate's leading edge, Re_x , of 1×10^5 are shown in Figures 15, 16, and 17 along with the exact solution given in Schlichting [15]. Solutions at Reynolds numbers of 0.8×10^5 , 1.6×10^5 , 2×10^5 , 2.4×10^5 , and 3.2×10^5 were also calculated. They produced results equivalent to those presented here and are not shown. As can be seen from these figures, there is excellent agreement between the calculations and the exact solution. The calculated values are accurate to within 1% of the exact values close to the wall ($y = 0$). The calculated velocity profile (Figure 16) has a maximum error of less than 2% at $y \sqrt{U_o / (\nu x)} = 4$. The calculated transverse velocity (Figure 17) has approximately a 4% error at $y \sqrt{U_o / (\nu x)} = 4$ and is less than 2% low at $y \sqrt{U_o / (\nu x)} = 8$.

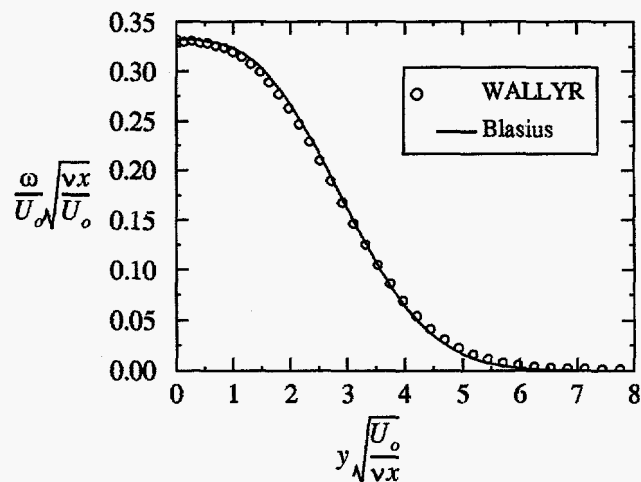


Figure 15. Blasius Vorticity Distribution

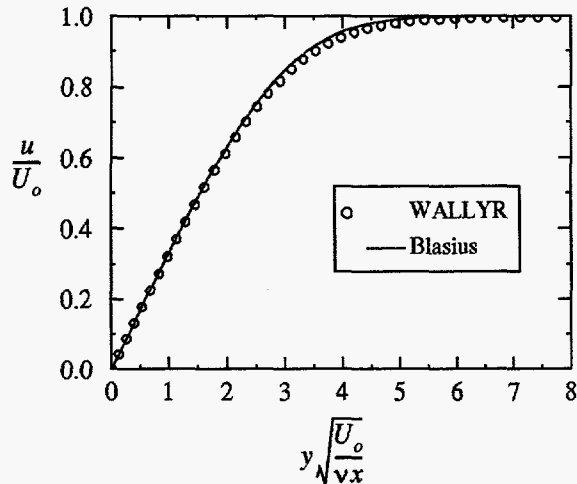


Figure 16. Blasius Velocity Profile

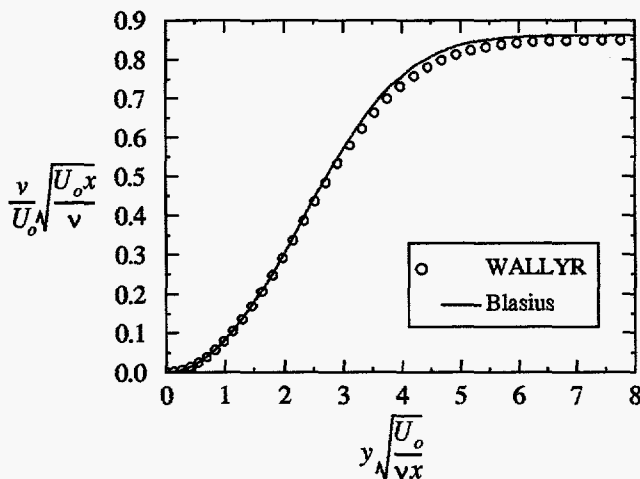


Figure 17. Blasius Transverse Velocity Profile

SUMMARY

A summary of the work completed to date and the work which should immediately follow is given below.

- We have demonstrated the use of the diffusion velocity concept in simple boundary layers where the diffusion is normal to the wall. The calculations show that excellent results can be obtained using this method.
- An accurate algorithm for representing the flux and distribution of vorticity generated at the wall during a given time step has been developed.

- Due to the linear nature of the diffusion equations we can treat the diffusion of oppositely signed vorticity separately and thus do not have to deal with the conceptually difficult situation where the vorticity is zero while the gradient of vorticity is not.
- "Diffusion boundaries" across which existing vorticity cannot flow are easily produced by using images of the vorticity distribution.
- We have demonstrated that good results are obtainable for simple zero pressure gradient flat plate flows.
- There is a need to continue this work by investigating simple boundary layer simulations with outer free blobs.
- We also need to investigate more complicated boundary layer flows such as flows with pressure gradients and separating flows.

REFERENCES

- [1] Spalart, P. R., Leonard, A., and Baganoff, D., "Numerical Simulation of separated Flows," NASA TM 84328, February 1983.
- [2] Spalart, P. R., "Vortex Methods for Separated Flows," NASA TM 100068, June 1988.
- [3] Chorin, A. J., "Numerical Study of Slightly Viscous Flow," *J. Fluid Mech.*, vol. 57, pp. 785-796, 1973.
- [4] Leonard, A., "Vortex Methods for Flow Simulation," *J. Comput. Phys.*, vol. 37, pp. 289-335, 1980.
- [5] Fishelov, D., "A New Vortex Scheme for Viscous Flows," *J. Comput. Phys.*, vol. 86, pp. 211-224, 1990.
- [6] Ogami, Y. and T. Akamatsu, "Viscous Flow Simulation using the Discrete Vortex Model-The Diffusion Velocity Method," *Computers & Fluids*, vol. 19, pp. 433-441, 1991.
- [7] Kempka, S. N. and Strickland, J. H., "A Method to Simulate Viscous Diffusion of Vorticity by Convective Transport of Vortices at a Non-Solenoidal Velocity," Sandia Laboratory Report SAND93-1763, December 1993.
- [8] Chorin, A. J., "Vortex Sheet Approximation of Boundary Layers," *J. Comput. Phys.*, vol. 27, pp. 428-442, 1978.
- [9] Koumoutsakos, P., Leonard, A., and Pepin, F., "Boundary Conditions for Viscous Vortex Methods," *J. Comput. Phys.*, vol. 113, pp. 52-61, 1994.

- [10] Carrier, J., Greengard, L., and Rokhlin, V., "A Fast Adaptive Multipole Algorithm For Particle Simulations," *J. Sci. Stat. Comput.*, vol. 9, no. 4, pp. 669-686, July 1988.
- [11] Currie, I. G., *Fundamental Mechanics of Fluids*, McGraw-Hill, pp. 231-237, 1974.
- [12] Kempka, S. N. and Strickland, J. H., "Velocity and Outflow Boundary Conditions for Vorticity Formulations," Sandia Laboratory Report SAND94-1735, January 1995.
- [13] Wu, J. Z., Wu, X. H., Ma, H. Y., Wu, J. M., "Dynamic Vorticity Condition: Theoretical Analysis and Numerical Implementation," *International Journal. for Numerical Methods in Fluids*, vol. 19, pp. 905-938, 1994.
- [14] Panton, R., "The Transient for Stokes's Oscillating Plate: A Solution in Terms of Tabulated Functions," *J. Fluid Mech.*, vol. 31, pp.819-825, 1968.
- [15] Schlichting, H., "*Boundary Layer Theory*," McGraw-Hill, pp. 125-129, 1968.

DISCLAIMER

This report was prepared as an account of work sponsored by an agency of the United States Government. Neither the United States Government nor any agency thereof, nor any of their employees, makes any warranty, express or implied, or assumes any legal liability or responsibility for the accuracy, completeness, or usefulness of any information, apparatus, product, or process disclosed, or represents that its use would not infringe privately owned rights. Reference herein to any specific commercial product, process, or service by trade name, trademark, manufacturer, or otherwise does not necessarily constitute or imply its endorsement, recommendation, or favoring by the United States Government or any agency thereof. The views and opinions of authors expressed herein do not necessarily state or reflect those of the United States Government or any agency thereof.
